Production of N_2^+ first negative emission by impact of 1-MeV H^0, H^+, and H^- on N_2

Redus F. Holland, Donald D. Cobb, William B. Maier II,
William B. Clodius, and P. G. O'Shea
Los Alamos National Laboratory, Los Alamos, New Mexico 87545

Randy Bos and Brent C. Frogget
EG&G, Energy Measurements Operations, Los Alamos, New Mexico 87544
(Received 15 May 1989)

Absolute cross sections for the production of photons in the N_2^+ first negative (0-0) and (0-1) bands by collisions of 1-MeV H^0, H^-, and H^+ on N_2 have been measured. The (0-0) cross sections are, respectively, 0.091 ± 0.03, 0.19 ± 0.06, and 0.15 ± 0.05 Å^2 per N_2 molecule, for H^0, H^-, and H^+ projectiles. The (0-1) cross section is 0.060 ± 0.02 Å^2 per N_2 molecule for H^- projectiles. Pressure dependences are observed in the apparent cross sections for $H^0+N_2\rightarrow 391$ nm and $H^-+N_2\rightarrow 391$ nm, at nitrogen pressures below 3.5×10^{-4} torr, and are ascribed to stripping of electrons from H^0 and H^-. The cross section for $H^-+N_2\rightarrow H^0+\cdots$ is measured to be $6.8(+2.3,-2.9)$ Å^2 per N_2 molecule. Where data for comparison exist, our measured cross sections are a factor of 2 or more higher than previously reported values.

I. INTRODUCTION

This paper reports absolute cross sections measured for the production of 391- and 428-nm N_2^+ first negative (1N) radiation by collisions of 1-MeV H^+, H^-, and H^0 with N_2. We also obtain a cross section for $H^-+N_2\rightarrow H^0+\cdots$ for H^- with a kinetic energy of 1 MeV.

The motivation for undertaking these measurements is twofold. First, collisions of H^0, H^-, and H^+ with N_2 have been studied experimentally several times,[1–4] and the cross sections for processes which strip electrons from H^- or H^0 are summarized by Tawara and Russek;[5] however, cross sections for the production of first negative emissions have not been reported at 1 MeV. Second, cross sections for the production of N_2^+ (1N) radiation by collisions between N_2 and 1-MeV H^+, H^-, and H^0 are needed to plan the BEAR (beam experiments aboard a rocket) space test of a neutral particle beam accelerator and to interpret some of the data collected during the test.[6]

The present data were obtained at the BEAR ground test facility at Los Alamos.[7]

II. EXPERIMENTAL PROCEDURES

A. Collision chamber configurations

A schematic diagram of the experimental setup is shown in Fig. 1. Briefly, a 1-MeV H^- beam from the accelerator passes through a neutralizing gas cell, where electrons are stripped from some of the projectiles. The beam, consisting of H^0, H^-, and H^+, emerges from the neutralizer, passes through an electromagnet that separates the differently charged components of the beam and directs them into a collision chamber containing nitrogen gas, past different observation windows, and into Faraday cups. An optical detector measures the light emerging through each of the windows, and cross sections are then computed from the beam path length within the field of view of the detector, the number of projectiles, and the known pressure within the collision chamber.

The current of H^- entering the neutralizer chamber ranged from roughly 4–20 mA during each of the 50-μs-long pulses from the accelerator. The fluxes of H^-, H^0, and H^+ depended on the pressure of xenon gas in the neutralizer. We typically operated with H^0:H^+:H^- $\sim$2:1:1, i.e., with a few milliamperes of each species. The energy spectrum of the H^- beam entering the neutralizer was measured with a magnetic spectrometer. The bending magnet was a 45° stigmatic homogeneous field electromagnet with rotated poles. The resolution of the spectrometer was 0.005 MeV at 1 MeV. A typical energy distribution is shown in Fig. 2.

The neutralizer and separation magnet can be operated so that the beam passing the center observation window contains all three charged components, only H^0, or only H^-. The magnet can deflect H^- and H^+ into either the upper or lower Faraday cups. These possibilities were variously permuted during the experiment without significant systematic effect on the results.

Pressure was measured with a MKS spinning rotor pressure gauge at two locations, separated by the length of the collision chamber. Indicated pressures at the two locations differed by $<1\%$. The calibration of the spinning rotor gauge was cross-checked between 10^{-3} and 5×10^{-5} torr against a MKS Baratron gauge which the manufacturer claimed was calibrated against a National Bureau of Standards (NBS)-traceable standard. The spinning rotor gauge was also checked against a local MKS spinning rotor gauge which was calibrated at NBS and was therefore a secondary pressure standard. These calibrations agreed within 12%; an average pressure calibra-

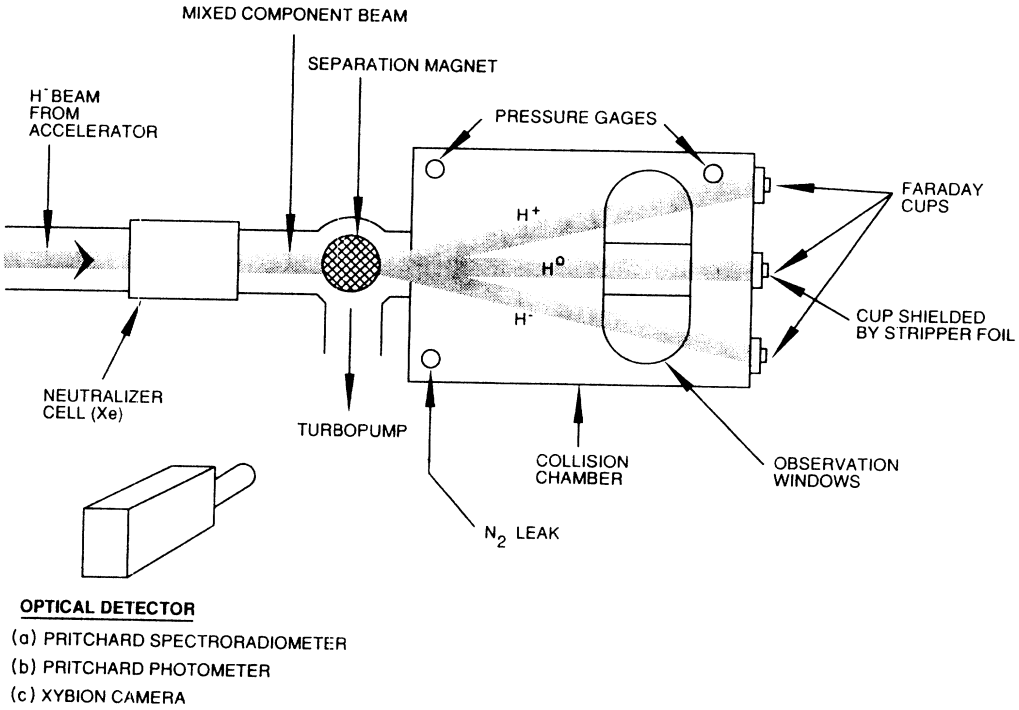

FIG. 1. Schematic diagram of the apparatus. The optical detector views ≈ 7.0 cm of the beam within the collision chamber through the observation windows. The separation magnet can be adjusted to pass H^+ or H^- through the upper or lower windows. All three beam components can be permitted to pass simultaneously along the path marked H^0.

tion was used, so the error associated with pressure uncertainty should be $\leq \pm 6\%$.

The base pressure within the collision chamber was about 5×10^{-6} torr. When the beam neutralizer was on, xenon gas diffused from the neutralizer into the collision chamber and raised the indicated pressure to about 1.2×10^{-5} torr.[8] During the cross-section measurements, spectral grade nitrogen was bled into the collision chamber, and measured N_2 partial pressures ranged from roughly 1.5×10^{-5} to 7.3×10^{-4} torr.

The Faraday cups were guarded against loss of secondary electron current by electrostatic and magnetostatic suppression. The entrance to the middle cup was covered by a 1.5-μm-thick nickel stripper foil to remove electrons from H^- and H^0; the middle cup thus measured the total proton current in the beam after all electrons have been removed from H^0 and H^-. Since the accelerator operates in a pulsed mode, it was necessary to measure both current amplitude and pulse width. Uncontrolled variations in these two parameters during operation may account for much of the scatter observed in our data, but the uncertainty in the average product of current amplitude and pulse width for ≥ 100 pulses is probably within $\pm 10\%$. By contrast, the variation in the charge contained in a single beam pulse was about $\pm 20\%$ from the mean value.

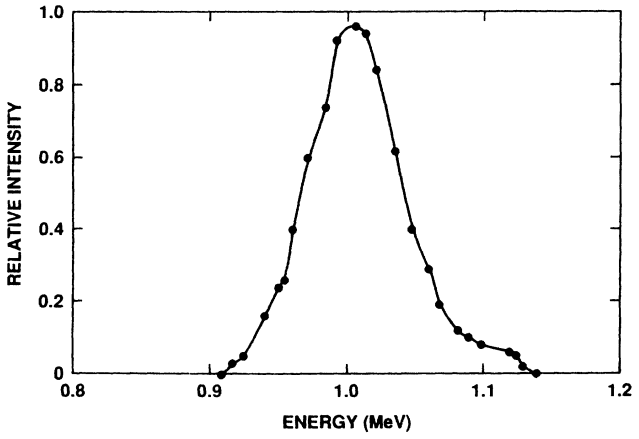

FIG. 2. Measured laboratory energy distribution for H^- in a single pulse from the BEAR ground test facility.

Current ranges during measurements of the cross sections, σ_{391}, for the production of 391-nm radiation were

H^0, 6.1–8.8 mA (equivalent) ;

H^+, 4.2–5.2 mA ;

H^-, 3.4–21.0 mA .

The current ranges for H^0 and H^+ were small for operational reasons, and dependences of σ_{391} on the currents of these two projectiles might not have been detected. Dependence of σ_{391} on the H^- current should have been easily observed. In any case, no systematic dependence of σ_{391} on projectile current was observed in these experiments.

Measurements with different optical detectors are described below. The collision chamber interior within the

field of view of the detectors was blackened to reduce reflections.

B. Measurements with the Pritchard detectors

Two Pritchard radiometers were used in these measurements. Both were operated as photometers with a suitably blocked interference filter [391 nm, 3-nm full width at half maximum (FWHM)] over the entrance optics.[9] One device was also used as a spectrally resolved radiometer with a nominal spectral resolution of 10 nm to obtain spectra between 370 and 440 nm. The Pritchard radiometers' field of view was 3°, corresponding to 7.0 cm of beam path. In each case, the optical detectors were calibrated against a diffuse source calibrator, which was itself several times calibrated by us against two NBS spectral radiance standard tungsten lamps. We used the calibration judged by us to be best, but all calibrations agreed with each other within 15% at the wavelengths of interest. We thus effectively calibrated three separate optical detectors with a device which was itself calibrated and cross checked against NBS standards.[10] The maximum uncertainty arising from the optical calibrations should be $< 15\%$ and could show up in the data as small systematic differences in data taken with different detectors.

In operation, light from the collision region was collected for a known time by the detector, and the signal was read from a digital display. Because light levels were comparable to the background drift of the Pritchard's output, it was necessary to make several consecutive observations of signal with and without light from chamber entering the detector. The drift of the detector's dark background signal introduced some scatter into the data but should introduce no systematic error into the cross sections.

A very small amount of visible background light was found to originate in the Faraday cups and was diffusely scattered into the optical detector's field of view. This light was too weak to be detected by our apparatus at 391 nm and was subtracted from the signals at all wavelengths where it was measurable.

Visual observations and the charge injection device (CID) camera measurements described in Sec. II C indicate that the vast majority of light entering the optical detectors originates in a well-defined region containing the projectile beam. Specifically, visible light reflected off of surfaces behind the beam or scattered by window surfaces appears to be dominated by the very weak light which originates in the Faraday cups and which is at least an order of magnitude less strong than the light from the beam. CID camera observations with the 391-nm filter described below measured identical backgrounds away from the well-defined beam with camera shutter open or closed and the projectile beam on or off.

The wavelength scale of the Pritchard spectroradiometer was calibrated against a mercury penlight, and all data herein have been corrected to the proper wavelength.

C. Measurements with the image-intensified CID camera

Images of the beam were recorded with a blue-enhanced, image-intensified, time-gated CID camera manufactured by Xybion Electronics Corp. The camera optics included a 50-mm, $f/0.95$ lens and a blocking interference filter (391 nm, 10-nm FWHM). The camera's viewing geometry was similar to that of the photometers (Fig. 1). The length of beam viewed by the camera was 12 cm. The beam diameter measured by the camera was 22 mm. The video output of the camera was recorded on video tape for off-line analysis.

During data acquisition the camera was externally synchronized to the beam-firing pulse supplied by the BEAR flight electronics system. The camera intensifier gate opened 4 μs before the beam appeared and closed a minimum of 6 μs after the beam pulse ended; several gate widths were used.

The camera's response was calibrated with a *pulsed* diffuse-light source. This light source was calibrated with one of the Pritchard photometers mentioned in Sec. II B. The calibration of this particular Pritchard photometer was checked against a Gamma Scientific Corporation NBS-traceable standard radiation source and was within 10% of the calibration which was actually used to reduce the beam data and which effectively provided the standard against which the CID camera response was calibrated.

The images recorded on videotape were analyzed in the following manner. First, 20 images of the H^- beam at each pressure were digitized and registered. Next, the camera-generated background shading was subtracted from each image. The 20 processed images were then averaged to produce a composite beam image. From this composite image and the camera calibrations we obtained a measurement of beam optical emission in J/cm^2 sr. The H^- cross sections reported here for the camera data were obtained from these measurements, along with measurements of the H^- beam current and the N_2 gas density in

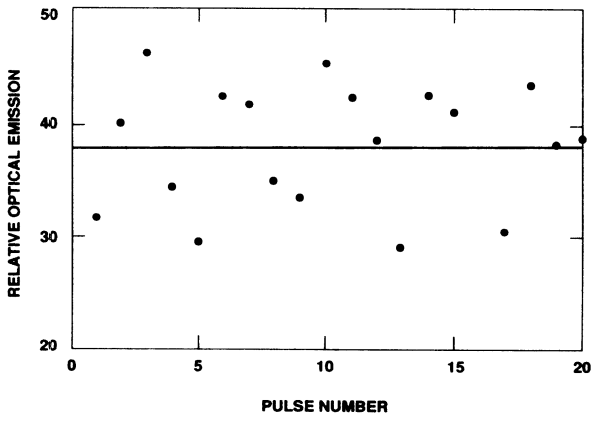

FIG. 3. Variation in the optical emission measured with the CID camera when the H^- beam passed through 2.74×10^{-4} torr of nitrogen. There was no Xe gas in the neutralizer, and the beam was directed into the middle Faraday cup. Data are shown as closed circles and the horizontal line is the average value.

the collision cell. The error bars associated with each data point are a combination of the variation obtained from the calibration of the camera, the variation in the measured optical emission of each image, and the uncertainty in the average beam current for each set of pulses. Figure 3 shows the variation in optical emission of consecutive pulses for twenty pulses. The primary source of variability is believed to be pulse-to-pulse variations in beam current.

III. EXPERIMENTAL RESULTS

Measured apparent cross sections for producing 391-nm light are shown in Figs. 4–6. The variation of these cross sections with nitrogen pressure will be discussed in Sec. IV. We take the true cross sections to be the extrapolated values at zero pressure. The two sets of data in Fig. 6 seem to be systematically displaced, and have been individually extrapolated to zero; the cross section is then taken to be the average of the zero-pressure values. Errors caused in these extrapolated values by irreproducibility are estimated from the data to be less than ±10%. Data obtained with the different optical detectors are distinguished on the figures and appear to be reasonably consistent with each other. We estimate systematic error in the cross sections to be within ±25%. The total uncertainty in the cross sections is thus about ±35%.

Data from the CID camera are also presented in Fig. 4, along with error bars representing the standard deviation in the scatter of data taken with the CID camera plus a ±25% uncertainty arising from the beam current determination for the camera observations only. The CID camera data lie below the Pritchard data, but the error bars in the CID data overlap the scatter in the Pritchard data. In addition to the uncertainties shown in Fig. 4, the CID data have associated systematic uncertainties similar to the Pritchard data. The cross sections quoted in this paper are based primarily on the Pritchard data.

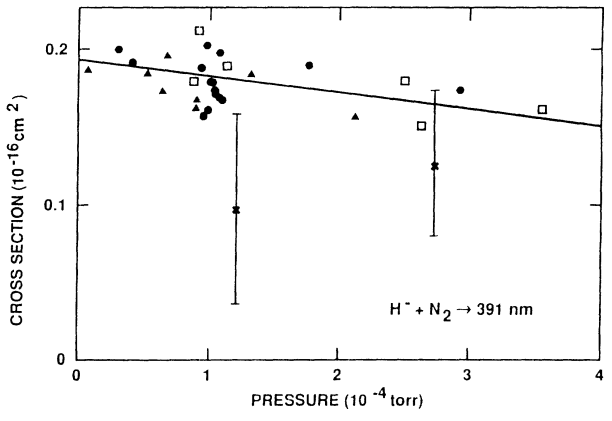

FIG. 4. Plot of the cross section for production of 391-nm light by H^- impact on N_2 vs nitrogen partial pressure. The symbols indicate data points: □, Pritchard S1118 operated as a spectroradiometer with 10-nm resolution; ▲, Pritchard S1118 operated as a photometer with 3-nm bandwidth; ●, Pritchard C971 operated as a photometer with 3-nm bandwidth. The line is a visually adjusted representation of the data. CID camera data are represented by ×, with error bars indicating uncertainty caused by reproducibility as described in Sec. III.

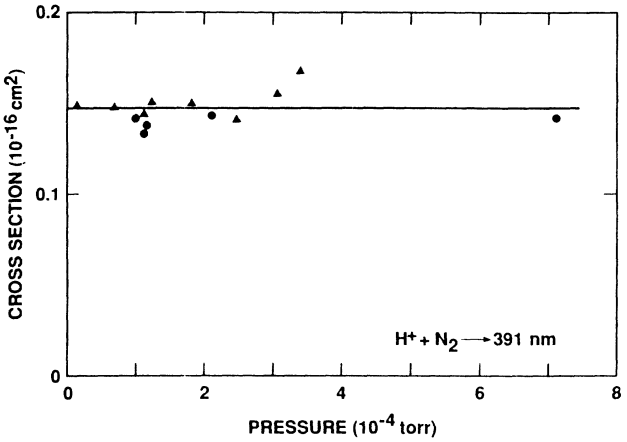

FIG. 5. Plot of the cross section for production of 391-nm light by H^+ impact on N_2 vs nitrogen partial pressue. The symbols indicate data points as in Fig. 4. The line is a visually adjusted representation of the data.

The spectral region from 370–440 nm was scanned with 10-nm resolution in 5-nm steps. The resulting spectrum is shown in Fig. 7, where the data points have been connected by straight lines. Spectral data from an earlier run on a different day are also shown for comparison. Maxima in the measured emissions occur near 391 nm, as expected for 1N(0-0), and near 425 nm, which is somewhat removed from the expected wavelength, 428 nm, for 1N(0-1).

During these experiments we observed that the H^- current measured by the lower Faraday cup decreased as the nitrogen pressure was increased. Table I gives three observed ratios for H^- current when the nitrogen pressure in the collision chamber was low and when it was raised to approximately 10^{-4} torr. From the estimated

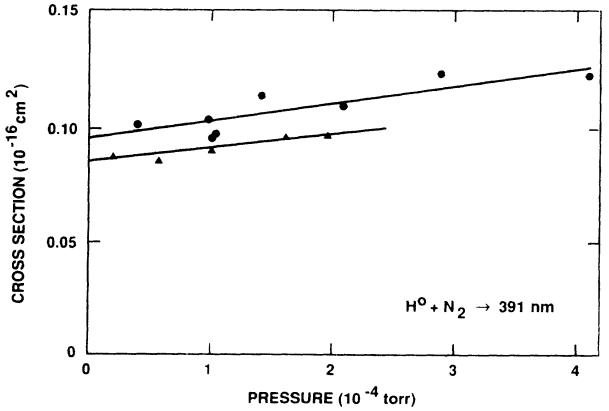

FIG. 6. Plot of the cross section for production of 391-nm light by H^0 impact on N_2 vs nitrogen partial pressure. The symbols indicate data points as in Fig. 4. The lines are visually adjusted representations of the data.

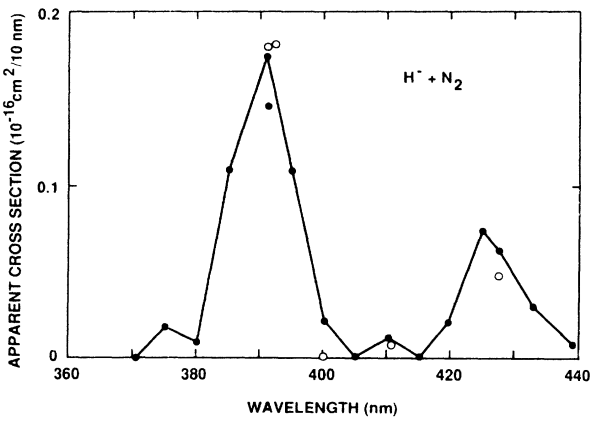

FIG. 7. Emission spectrum produced by 1-MeV H^- passing through nitrogen at about $2.5\pm0.1\times10^{-4}$ torr. The symbols (● and ○) show data points for different runs. The instrumental resolution is 10 nm. The solid circles are connected by lines merely to provide visual continuity.

effective length of the collision chamber (78±8 cm), the pressure, the change in indicated current, and the assumption that the decrease in H^- current is caused by $H^-+N_2\rightarrow H^0+\cdots$, we calculate the stripping cross section $\sigma_s(H^-)$ given in Table I. (The effective length of the collision chamber differs slightly from its actual length because of fringing fields of the separation magnet and because of pressure drop across the region between the collision chamber and the turbo pumped volume.) Possible sources of systematic error in our values are uncertainties in the effective path length times pressure, possible changes in the functioning of the Faraday cup at different pressures, and errors in the pressure measurement. Collisions which take H^- or H^0 to H^+ before the beam reaches the Faraday cup further reduce the indicated H^- current and effectively increase the computed stripping cross section; at 10^{-4} torr we estimate that $H^++N_2\rightarrow H^-+\cdots$ causes less than 5% error in $\sigma_s(H^-)$. The error caused by $H^0+N_2\rightarrow H^+\cdots$ depends on the size of this process's cross section, $\sigma_s(H^0)$, which has been previously reported to be[5] 1.5 Å^2/N_2 and is estimated later in this paper to be 6.2±4 Å^2/N_2; if $\sigma_s(H^0)=1.5$ Å^2/N_2, then the error in $\sigma_s(H^-)$ is <4%, but if $\sigma_s(H^0)=6.2$ Å^2/N_2, then $\sigma_s(H^-)$ is too large by about 16%. The absolute accuracy of the beam current measurement is of no import. We estimate the other systematic errors in our measured stripping cross sections to be $\leq\pm20\%$. Table I gives $\sigma_s(H^-)=6.8$ Å^2/N_2 from our data, and our total range of uncertainty indicates that the true value for $\sigma_s(H^-)$ should be between 3.9 and 9.1 Å^2/N_2.[11]

TABLE I. Cross section, $\sigma_s(H^-)$, per N_2 molecule for $H^-+N_2\rightarrow H^0+\cdots$ with 1-MeV H^-.

Nitrogen pressure (10^{-4} torr)	H^- current[a] ratio	Cross section (Å^2)[b]
0.986	$\frac{14.5}{17.5}$	7.61
0.976	$\frac{15.0}{17.6}$	6.57
0.956	$\frac{15.5}{18.0}$	6.23
Average cross section		6.81±0.8[c]
Previously published value		3.2 ±1.4[d]

[a]The ratio shown is H^- current in mA for $P\approx10^{-4}$ torr divided by H^- current for $P\approx0$.
[b]1 Å$=10^{-8}$ cm.
[c]The error here is based on reproducibility. When systematic uncertainty is considered, the true value may be as much as 41% larger or 25% smaller than 6.8 Å^2 (see Ref. 11).
[d]Reference 5. We have estimated this uncertainty from the scatter in the data.

Emitted light was also measured when the neutralizer (Fig. 1) was operating and the field in the separation magnet was zero. In this circumstance, the H^+, H^-, and H^0 components remained as a single beam that was directed into the central Faraday cup. The optical power, L, produced by the beam in the field of view of the detector was then the sum of the light produced by each component,

$$L=n(\sigma_+I_++\sigma_-I_-+\sigma_0I_0)l\ , \tag{1}$$

where n is the number of N_2 molecules/cm^3; $\sigma_{\pm,0}$ is the cross section for production of light by H^+, H^-, and H^0; l is the path length within the optical detector's field of view; and $I_{\pm,0}$ is the number of H^+, H^-, and H^0 passing through the detector's field of view per unit time. The current I measured by the central Faraday cup was $I=I_++I_-+I_0$. Composite cross sections, σ, for production of 391-nm radiation from the composite beam were computed from

$$\sigma=\frac{L}{nlI} \tag{2}$$

and are given in Table II. Because the cross sections in Figs. 4–6 for individual beam components exhibit pressure dependences, σ also will show a dependence on pressure.

TABLE II. Composite cross sections, σ, per N_2 molecule for 391-nm light produced by composite beams for two cases.

I[a] (mA)	Pressure (torr)	Observed[b] σ (Å^2)	Predicted[c] σ (Å^2)
16.8	1×10^{-4}	0.115	0.127
13.1	1.1×10^{-4}	0.167	0.137[d]

[a]I is the total proton current measured by the middle Faraday cup, after the electrons have been stripped from all components by the stripping foil. The sum of the measured component currents may differ slightly from I because of temporal variation in accelerator output or differences in Faraday cups.
[b]Computed from Eq. (2).
[c]Computed from $\sigma=(1/Il)(L_+/n_++L_0/n_0+L_-/n_-)$, where $L_{\pm,0}$ and $n_{\pm,0}$ are, respectively, the light intensity and N_2 number densities corresponding to the measured $I_{\pm,0}$. Values of $I_{\pm,0}$ were obtained several minutes apart, and the nitrogen pressure varied slightly (<10%).
[d]L_-, n_-, and I_- were not separately measured, so we used $I_-=I-I_0-I_+$ and took $L_-/n_-=(L_-/n_-)_p(I_-/I_{p-})$, where the subscript p denotes a previous measurement.

IV. DISCUSSION

Despite the diversity of instruments used to measure the cross section for production of radiation near 391 nm, the data from different devices are reasonably consistent. Such agreement eliminates detector-dependent systematic errors as sources of large uncertainties in the observations. On the other hand, obtaining cross sections for the production of N_2^+ (1N) bands from the data requires some interpretation of the observations.

First, the low-resolution spectrum in Fig. 7 indicates that there is no general background of radiation confusing the interpretation of the data. The prominent spectral features in Fig. 7 disappear if the N_2 is removed from the collision chamber. The spectral features near the 1N(0-0) band at 391 nm and 1N(0-1) band at 428 nm may nevertheless involve contributions from other bands of N_2. Contributions from these bands will cause the cross sections to appear higher than the true values; the size of the effect can be estimated from the spectrum in Fig. 7, from available branching ratios, and from previously published spectra.[1,4,12–15] Published spectra indicate that the 1N(0-0) and 1N(0-1) bands will be the major contributors to the prominent spectral features in Fig. 7. The peak of the strongest feature is appropriately close to 391 nm, but the peak of the feature near the 1N(0-1) band lies near 425 nm rather than 428 nm, where the (0-1) band should be. Thus, it appears that the cross section for the (0-1) band may be appreciably influenced by other bands.

Contributions from the N_2 second positive (2P) system are hard to estimate precisely, because previous, suitable spectroscopic data for 1-MeV $H^{0,\pm}$ are unavailable. The data which do exist at lower projectile energies suggest that the influence of $N_2$2P bands on our results is small, and our data are consistent with this expectation.[1–4]

We can estimate contributions to the spectral features near 428 and 391 nm from the other N_2^+ 1N bands from the branching ratios and the *assumption* that the $N_2^+(B)$ vibrational population is similar to populations produced by electron impact:

B-state vibrational level	Population (Ref. 13)
0	0.885
1	0.103
2	0.0083
3	0.0036

These populations, the branching ratios in Table III, and the spectral passband of the optical detectors are combined to produce the following correction factors. For the Pritchard photometers,

$$\sigma_{0\text{-}0}(\text{true}) \approx 0.996\sigma_{391}(\text{observed}) .$$

For the Pritchard spectroradiometer,

$$\sigma_{0\text{-}0}(\text{true}) \approx 0.97\sigma_{391}(\text{observed}) , \quad (3)$$

$$\sigma_{0\text{-}1}(\text{true}) \approx 0.92\sigma_{428}(\text{observed}) , \quad (4)$$

$$\sigma_{0\text{-}1}(\text{true}) \approx 0.86\sigma_{425}(\text{observed}) .$$

TABLE III. Bandhead wavelengths λ and branching ratios b for the N_2^+ first negative bands. V' is the vibrational quantum number of upper state and V'' is the vibrational quantum number of lower state.

V'	V''	$\lambda(V',V'')$ (Å)	$b(V',V'')$[a]
0	0	3914	0.7050
	1	4278	0.2304
	2	4709	0.0529
	3	5228	0.0099
	4		0.0016
	5		[0.0002]
1	0	3582	0.3309
	1	3884	0.2794
	2	4236	0.2577
	3	4651	0.0991
	4	5148	0.0260
	5		[0.0056]
2	0		0.0706
	1		0.4545
	2		0.0736
	3		0.2183
	4		0.1316
	5		0.0514

[a]Skumanich and Stone, Ref. 18, from data in Refs. 19 and 20. Quantities in brackets derived from Jain and Sahni, Ref. 21.

σ_{391}(observed) denotes the zero pressure extrapolated values in Figs. 4–6. We estimate σ_{428}(observed) from Fig. 7 and the pressure dependence in Fig. 4. Table IV lists our best cross sections for the production of light in the 1N(0-0) and 1N(0-1) bands.

From Table III, one calculates

$$\frac{\sigma_{0\text{-}0}}{\sigma_{0\text{-}1}} = \frac{0.7050}{0.2304} = 3.06 .$$

The cross sections in Table IV yield $\sigma_{0\text{-}0}/\sigma_{0\text{-}1} = 3.22 \pm 0.8$, within experimental uncertainty of the expected value.

The measured cross section, σ_{391}, in Fig. 5 for production of 391-nm radiation by $H^+ + N_2$ shows little or no dependence on pressure for pressure $< 7.3 \times 10^{-4}$ torr. By contrast, σ_{391} increases with increasing pressure for $H^0 + N_2$ and decreases for $H^- + N_2$. Our interpretation of these observations is that the pressure dependences arise from stripping of electrons from H^- and H^0. Thus, when an electron is stripped from H^- before reaching the field of view of the optical detector, the resulting H^0 projectile has a smaller cross section for exciting 391-nm emission, and the apparent cross section falls as pressure is increased. When an electron is stripped from H^0, the resulting H^+ projectile has a larger cross section for producing 391-nm radiation, and σ_{391} rises with increasing pressure. Because the cross section for a 1-MeV H^+ to pick up an electron is very small, the charge state of the H^+ beam is insensitive to pressure, and σ_{391} is also observed to be insensitive to pressure in our experiment.

If the above interpretation of the pressure dependences

TABLE IV. Cross sections per N_2 molecule for the production of a radiated photon in the 1N(0-0) (391 nm) and (0-1) (428 nm) bands by collisions of 1-MeV H^+, H^-, and H^0 with N_2.

Projectile	Present[a] cross sections ($Å^2$) 0-0[b]	0-1[b]	Previous values ($Å^2$) 391 nm[b]
H^+	0.148±0.05		0.07±0.025[c]
H^-	0.193±0.06	0.060±0.02[d]	
H^0	0.091±0.03		

[a]Corrected for estimated contributions for other N_2^+ 1N bands. Estimated systematic uncertainty is included in the quoted error. $1\ Å \equiv 10^{-8}$ cm.
[b]N_2^+ 1N band or wavelength associated with the emission.
[c]This value, estimated from data of Dufay *et al.* (Ref. 3), is below an estimate of Van Zyl *et al.* (Ref. 4) based on data on emission excited by electrons, and is above an extrapolation of the data of Thomas *et al.* (Ref. 2). The error is estimated from the data scatter in an illustration in Ref. 4.
[d]Inferred from Fig. 7 and the pressure dependence in Fig. 4.

in Figs. 4 and 6 is correct, then it should be possible to estimate stripping cross sections for H^- and H^0 from the slopes of the apparent cross sections. For the data in Fig. 4, the appropriate expression is

$$\sigma_s(H^-) \approx \frac{1}{Z(\sigma_0-\sigma_-)_{P=0}} \frac{d\sigma_-}{dn} , \tag{5}$$

where $\sigma_s(H^-)$ is the cross section for $H^- + N_2 \rightarrow H^0 + \cdots$, σ_- is the apparent cross section in Fig. 4, $Z = 58$ cm is the effective distance between the end of the separation magnet and the center of the observation window, and σ_0 is the cross section in Fig. 6. Now,

$$\frac{d\sigma_-}{dn} = \frac{1}{3.22\times 10^{16}} \frac{d\sigma_-}{dP} , \tag{6}$$

where P is the N_2 partial pressure in torr, $(\sigma_0-\sigma_-)$ in the denominator of Eq. (5) is the extrapolated value at $P=0$ (see Table IV), and $d\sigma_-/dP$ is read from the line in Fig. 4. A very similar expression to Eq. (6) gives $\sigma_s(H^0)$, the cross section for $H^0 + N_2 \rightarrow H^+ \cdots$, and we average the slopes of the two lines in Fig. 6 to obtain $d\sigma_0/dP$. The results are

$$\sigma_s(H^-) = 6.4 \pm 2.5\ Å^2/N_2 \tag{7}$$

$$\sigma_s(H^0) = 6.2 \pm 4\ Å^2/N_2 . \tag{8}$$

$\sigma_s(H^-)$ is well within experimental error of our measured value in Table I but still a factor of 2 higher than the previously reported value.[5] $\sigma_s(H^0)$ is a factor of 4 higher than the previously reported value,[5] 1.5 $Å^2/N_2$, and we have no other value for comparison; however, Tawara and Russek report $\sigma_s(H^-)/\sigma_s(H^0) \sim 2$ for several gases,[5] and our value of $\sigma_s(H^0)$ should be viewed with reservation.

The question arises whether some processes other than stripping of single electrons may be influencing the slopes of the lines in Figs. 4 and 6. Our estimates of the effect of stripping two electrons from H^- indicate that the effect is very small ($<5\%$). Another possibility is that emissions produced by secondary electrons increase the slopes of the lines in Figs. 4 and 6. Electrons produced in the neutralizer cell (Fig. 1) are removed from the beam prior to the collision chamber by a deflection magnet. Electrons produced in the collision chamber have up to 550 eV of energy and will produce N_2^+ 1N emissions. However, the number of secondary electrons produced within the field of view of the optical detector is far too small to influence the measured cross sections significantly at the pressures involved. Secondary electrons tend to be produced with scattering angles such that they leave the beam; hence, most secondary electrons produced outside of the detector's field of view do not produce radiation that can be observed by the detector.[16] If the correction for secondary electron effects decreased $\sigma_s(H^0)$ in Eq. (8), then it should increase $\sigma_s(H^-)$ in Eq. (7). We anticipate no experimentally significant effects from secondary electrons in our results.[17]

A test of the accuracy of our observations for the production of 391-nm light is the accuracy with which we can predict the emissions produced by a composite beam of H^+, H^-, and H^0 from the light excited by the individual components. Table II gives a comparison of measured and predicted emissions from composite beams. The agreement is not perfect but is probably within the combined experimental uncertainties (reproducibility, measurement of individual component equivalent currents, and beam and pressure variations).

As previously mentioned, the data available for direct comparison with our cross sections are sparse. Table I compares our cross section for $H^- + N_2 \rightarrow H^0 + \cdots$ with that found in Tawara and Russek;[5] our value is substantially higher. Similarly, our cross section for $H^+ + N_2 \rightarrow$ (391-nm photons) in Table IV is roughly twice the previously reported value, and the extreme values allowed by experimental uncertainties do not quite overlap. Thus, there may be significant differences between our cross sections and those previously reported, but there may be no irreconcilable discrepancies, because previous data are sparse and rather scattered.

Specifically, we know of no measurements for the pro-

duction of N_2^+ 1N emission by 1-MeV $H^{0,\pm}$. The previous value for σ_{391} in Table IV is an extrapolation of the data of Dufay *et al.*[3] from 600 keV. Several measurements for production of σ_{391} by 100-keV H^+ gives values which differ from Dufay's results at 100 keV by roughly a factor of 2, both higher and lower. Hence at lower energies, where there are more measurements, the previous data are scattered.

Examination of the cross sections in Table IV shows that the charged species, H^- and H^+, have larger cross sections for producing N_2^+1N radiation than does H^0. Presumably, the larger cross sections are caused by a long-range force between N_2 and H^+ or H^-. Whether the larger cross section for H^- than for H^+ has significance is unclear from our data; specifically, on the basis of $\pm 10\%$ reproducibility for each cross section, we calculate the ratio of cross sections

$$\frac{\sigma_{0\text{-}0}(H^-)}{\sigma_{0\text{-}0}(H^+)} = 1.3 \pm 0.26 ,$$

which nearly allows the interpretation that $\sigma(H^-) \approx \sigma(H^+)$, if the full range of experimental uncertainty is invoked. On the other hand, it is certainly possible that $\sigma(H^-) > \sigma(H^+)$, as our data suggest.

V. SUMMARY

We have measured cross sections for production of the N_2^+ 1N(0-0) band at 391 nm by impact of 1-MeV H^-, H^+, and H^0 on N_2 and have obtained the cross section for the $H^- + N_2 \rightarrow N_2^+$ [1N(0-1)]. These cross sections are presented in Table IV. Our data also give a value for the stripping of an electron from H^- to give H^0 (see Table I). The cross section $\sigma_s(H^0)$ *estimated* for $H^0 + N_2 \rightarrow H^+ + \cdots$ from the pressure dependence in Fig. 6 is subject to larger systematic uncertainties than our other cross sections. Cross sections for $H^+ + N_2 \rightarrow$ 391-nm photons and for the stripping process $H^- + N_2 \rightarrow H^0 + \cdots$ are roughly a factor of 2 higher than previously reported results. The ranges of values within our estimated uncertainties either overlap or almost overlap the ranges in previous values.

ACKNOWLEDGMENTS

The authors are pleased to acknowledge the excellent support provided by the BEAR ground test facility team. Gordon Smith provided calibrated pressure gauges, spectral grade N_2, and gas handling system. This work was performed for the U.S. Department of Defense, Strategic Defense Initiatives Office, under the auspices of the U.S. Department of Energy.

[1] J. H. Birely, Phys. Rev. A **10**, 550 (1974).

[2] E. W. Thomas, G. D. Bent, and J. L. Edwards, Phys. Rev. **165**, 32 (1968).

[3] M. Dufay, J. Desesquelles, M. Druetta, and M. Eidelsberg, Ann. Geophys. **22**, 614 (1966).

[4] B. Van Zyl, M. W. Gealy, and H. Neumann, Phys. Rev. A **28**, 2141 (1983).

[5] H. Tawara and A. Russek, Rev. Mod. Phys. **45**, 178 (1973).

[6] BEAR is an acronym for Beam Experiment Aboard Rocket. The payload should attain a maximum altitude of about 200 km and should eject 5-mA H^+, 5-mA H^-, and 10-(mA/*e*) H^0 pulses 50 μs long at 5 Hz. The planned particle energies are 1 MeV. See T. M. Foley, Aviat. Week Space Technol. **128**(12), 70 (1988).

[7] P. G. O'Shea, D. L. Schrage, L. M. Young, T. J. Zaugg, M. T. Lynch, K. F. McKenna, and L. D. Hansborough, Nucl. Instrum. Methods **B40/41**, 946 (1989).

[8] Because of the way the spinning rotor gauge works, the true pressure of Xe in the collision chamber is a factor of 4–5 lower than 1.2×10^{-5} torr.

[9] The effective transmittance of the interference filter for the 391-nm (0,0) band was 28.5%, as determined from the measured filter transmittance and a band profile calculated for 298 K rotational temperature.

[10] A current manufacturer's calibration for one Pritchard photometer indicated an instrumental sensitivity 16% higher than the calibrations which we performed and used at wavelengths of interest. One of the Pritchard photometers was also calibrated against another NBS-traceable standard; see Sec. II C.

[11] When combining systematic error with "random" uncertainty arising from scatter in the data, we held the *fractional* "random" uncertainty constant and multiplied both the value of $\sigma_s(H^-)$ and its fractional "random" uncertainty by a single number. The absolute random uncertainty thus obtained is added to or subtracted from $\sigma_s(H^-)$ to obtain the experimentally allowed range of $\sigma_s(H^-)$.

[12] J. H. Moore, Jr. and J. P. Doering, Phys. Rev. **177**, 218 (1969).

[13] P. N. Stanton and R. M. St. John, J. Opt. Soc. Am. **59**, 252 (1969).

[14] J. L. Dunn and R. F. Holland, Los Alamos Scientific Laboratory Report No. LA-4314, 1969 (unpublished). Cf. J. L. Dunn and R. F. Holland, J. Chem. Phys. **54**, 470 (1971).

[15] R. F. Holland, Los Alamos Scientific Laboratory Report No. LA-3783, 1967 (unpublished).

[16] The CID images show emission from a sharply defined projectile beam.

[17] Two other possible sources of error are scattering of projectiles from the beam, which would cause an erroneous, low current reading, and collisional production of excited H^0 within the beam, which could alter the slopes of the lines in Figs. 4 and 6. Neither of these sources of error is expected to be significant; however, pertinent experimental data for a definitive statement are unavailable.

[18] A. Skumanich and S. Stone, unpublished results.

[19] L. Wallace, thesis, University of Western Ontario, 1954.

[20] L. V. Wallace and R. W. Nicholls, J. Atmos. Terr. Phys. **24**, 749 (1962).

[21] D. C. Jain and R. C. Sahni, Int. J. Quant. Chem. **1**, 721 (1967).

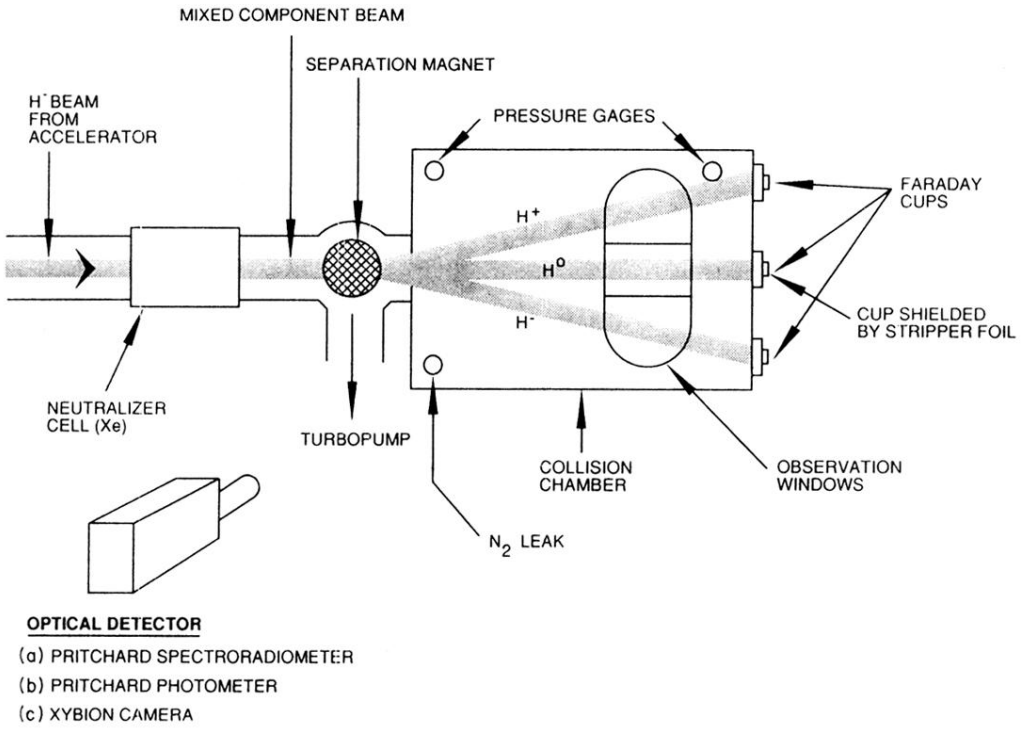

FIG. 1. Schematic diagram of the apparatus. The optical detector views ≈ 7.0 cm of the beam within the collision chamber through the observation windows. The separation magnet can be adjusted to pass H^+ or H^- through the upper or lower windows. All three beam components can be permitted to pass simultaneously along the path marked H^0.